ARTICLES

Hit-and-run planetary collisions

Erik Asphaug[1], Craig B. Agnor[1] & Quentin Williams[1]

Terrestrial planet formation is believed to have concluded in our Solar System with about 10 million to 100 million years of giant impacts, where hundreds of Moon- to Mars-sized planetary embryos acquired random velocities through gravitational encounters and resonances with one another and with Jupiter. This led to planet-crossing orbits and collisions that produced the four terrestrial planets, the Moon and asteroids. But here we show that colliding planets do not simply merge, as is commonly assumed. In many cases, the smaller planet escapes from the collision highly deformed, spun up, depressurized from equilibrium, stripped of its outer layers, and sometimes pulled apart into a chain of diverse objects. Remnants of these 'hit-and-run' collisions are predicted to be common among remnant planet-forming populations, and thus to be relevant to asteroid formation and meteorite petrogenesis.

Recent modelling[1] shows that for the random velocities expected[2,3] following the initial runaway-oligarchic stage of terrestrial planet growth[4–6], about half of giant impacts result in no net mass accumulation. In many cases, especially at grazing incidence, the impactor emerges disrupted (for example, ref. 7) but unaccreted. We focus on two principal consequences of impactor disruption: (1) unloading of a surviving planet-sized impactor from hydrostatic pressure over the encounter timescale (hours), which leads to fracture, igneous alteration, and possible melting and petrogenesis; and (2) density-driven material segregation, which occurs when impactors lose their outer layers owing to tides, shocks and shears.

From Roche encounters to hypervelocity collisions

Giant impacts, defined as collisions between planets of comparable size, range from grazing events (impact angle $\xi \approx 90°$; see Fig. 1), where gravitational stresses dominate, to direct hits ($\xi \approx 0°$), where shocks dominate. The best-studied giant impact of all, the proposed origin of the Moon (reviewed in refs 8 and 9), appears to require a collision of intermediate ξ and an impact velocity $v_{\rm imp}$ just barely above the two-body escape velocity $v_{\rm esc} = \sqrt{2G(M+m)/(R+r)}$, where M and m are the masses of the colliding planets, G is the gravitational constant, and R and r are their radii. In one scenario[10], a Mars-sized planet (about half an Earth diameter, or about one-tenth an Earth mass, $M_\oplus$) collides with the proto-Earth at about $\xi \approx 45°$ and $v_{\rm imp} \approx 1.05 v_{\rm esc}$ and is sheared by gravitational and mechanical torques and shocked to high pressure. A protolunar disk consisting about equally of impactor mantle and target mantle is ejected, while the remainder (including nearly all the impactor's core) accretes. This segregation of rock from iron, which accounts in this scenario for the iron-poor Moon, is also observed in models of collisions that are non-accretionary, leading us to explore generally how giant impacts process and segregate unaccreted materials.

The end-member archetypes of planetary collisions are hypervelocity impacts and disruptive tidal encounters inside the Roche limit. Both end members were exhibited by comet Shoemaker–Levy 9 (S–L/9). Much smaller than Jupiter and half as dense (interloper radius $r \approx 1$ km and density $\rho_{\rm i} \approx 0.6\,{\rm g\,cm^{-3}}$; ref. 11), S–L/9 fragmented deep inside the Roche limit at periapse ($a = 1.31R \approx 0.4\,R_{\rm Roche}$) into ~20 gravitationally bound clumps, on 8 July 1992. Here $R_{\rm Roche} = 2.46R(\rho_{\rm t}/\rho_{\rm i})^{1/3}$ is the Roche limit for tidal disruption, R is the target radius (in this case Jupiter), and $\rho_{\rm t}$ and $\rho_{\rm i}$ are the target and impactor densities.

As luck would have it, after a two-year eccentric orbit about Jupiter S–L/9 became the one observed example of a planet-scale hypervelocity collision. The fragments of tidal disruption, now distributed as a 'string of pearls', came back and struck Jupiter at $\sim 60\,{\rm km\,s^{-1}}$, producing a series of large dark blemishes observable with backyard telescopes. The tidal break-up involved gravitational unloading over the course of hours and the formation of a distinctive family of comets; the impacts involved intense shock compression in a tenth of a second and a few billion tons of shock-evolved compounds added to Jupiter. For small interlopers such as comets, planetary encounters are generally 'hit or miss'. For larger impactors ($r \lesssim R$; see Fig. 1), on the other hand, there is a broad range of intermediate outcomes we now explore.

Larger impactors

Tidal disruption can only happen to interlopers larger than a given size, for a given strength[12], so that if small comets commonly suffer tidal disruption[13] then one expects the process to be a common aspect of planet formation. But in late-stage giant impacts following runaway-oligarchic growth[4–6], impactors and targets are of comparable size, and cannot get deep inside the tidal field without colliding. It has therefore been argued that massive impactors escape tidal disruption[14]. However, massive impactors are observed in the calculations presented below to suffer profound tidal effects during giant impacts, in addition to profound shocks and mechanical shears—more so than their targets, which are notoriously difficult to disrupt by collision[44].

Massive impactors are much more easily disrupted than the targets they strike, for three reasons. (1) The ratio of tidal stress to self-gravitational stress between colliding bodies of masses m and M, of similar composition, varies inversely with mass, so the impactor bears the brunt of any tidal deformation. (2) Global shock intensities are concentrated in the impactor, approximately in proportion to its smaller volume, because shocks propagate about equally in both directions from the contact plane. (3) Strong mechanical shears, which arise because part of a giant impactor simply 'misses' the target (see Fig. 1), lead to differential stresses that are inversely proportional to the decelerated mass. Overall, an impactor half the size of a target will suffer disruptive consequences almost an order of magnitude more severe. Below we show case studies of typical planetary embryos colliding but not accreting: in many cases, the impactor becomes a novel planet or a family of novel planets, plus copious debris.

[1]Earth Sciences Department, Institute for Geophysics and Planetary Physics, 1156 High St, University of California, Santa Cruz, California 95064, USA.

Unloading

Planets possess great specific enthalpy in their compressed interiors. When a planet is disrupted, it unloads from gravitational equilibrium, which liberates significant quantities of internal energy separate from the kinetic energy of impact. For example, the ~20 fragments of S–L/9 exhibited prolific and energetic dust production[15], probably owing to the sudden exposure of volatile-rich interior surfaces released from an overburden pressure $P \approx 0.001$ bar. A planetary embryo, if disrupted by a similar process, would unload from pressures millions of times greater, and if rich in volatiles[16] might erupt. The energy per unit mass of the product of decompression[17] is $\int dP/\rho$, which for constant density (up to the onset of vaporization) is $\sim P/\rho \approx G\rho r^2$. Material unloaded from the base of a Mars-sized planet's mantle releases $\sim 2 \times 10^{10}$ erg g^{-1}, about the energy density of TNT.

Unlike shocks, which deposit energy locally, this unloading energy is available throughout the interior, leading to thermophysical events of different scale and character to those associated with impact shocks. The energy of unloading is proportional to the square of a disrupted planet's radius; unloading of a Neptune-mass planet's mantle would release over 10^{11} erg g^{-1}. In stellar encounters collisional unloading is particularly dramatic, for consideration regarding turn-of-the-century "planetesimal" concepts[18] of planet formation.

To evaluate the significance of pressure unloading in terrestrial collisions, we first simulate a purely tidal encounter with no shock pressures. We use the smooth particle hydrodynamics (SPH) code of Benz[19] to model a differentiated Moon-sized planet (70 wt% rock mantle, 30 wt% Fe core) suffering a close (non-impacting) encounter with a Mars-sized planet (Fig. 2a). The method and equation of state are those of ref. 10. Figure 2b plots the evolution of the interior pressure over the course of the encounter; the interloper experiences a transient global pressure drop of ~30–50%, from tides alone, for about an hour. Internal pressure recovers to only ~80% of its pre-encounter value because of spin-up and removal of the outer layers. Pressure release melting at a global scale might ensue if the

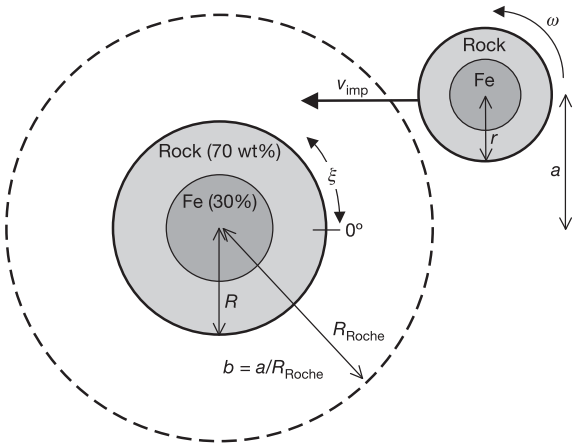

Figure 1 | Planetary embryos of comparable diameter are believed to have collided in giant impacts in the late stage of Solar System formation. This occurs following runaway-oligarchic growth[4–6]. We model colliding planets as differentiated, equilibrated bodies composed of 30 wt% iron cores surrounded by 70 wt% rocky mantles. Here R_{Roche} is the Roche limit (see text), ω is the rotation rate of the impactor (assumed zero in the calculations presented below), a is the closest approach of the encountering centres of masses (focusing included), v_{imp} is the impact velocity ($v_{imp}^2 \approx v_\infty^2 + v_{esc}^2$ where v_∞ is the velocity at infinity, that is, the random velocity of the encountering planets and $v_{esc} = \sqrt{2G(M+m)/(R+r)}$ is the two-body mutual escape velocity), M and m are the masses of the planets, R and r are their radii, and ξ is the angle of first contact for undeformable homogeneous spheres, where 90° is grazing, 0° is head-on. Although the usual rule applies that $\xi = 45°$ is the most probable, there is an important scale difference relative to better-studied[7] cratering events. When $r \approx R$, half of a 45° impactor 'misses' the planet, whereas when $r \ll R$ all of a 45° impactor collides (a typical cratering event). Planets are gravitationally compressed before our simulations, so that bulk density ρ is slightly greater for the planet with the larger mass, M.

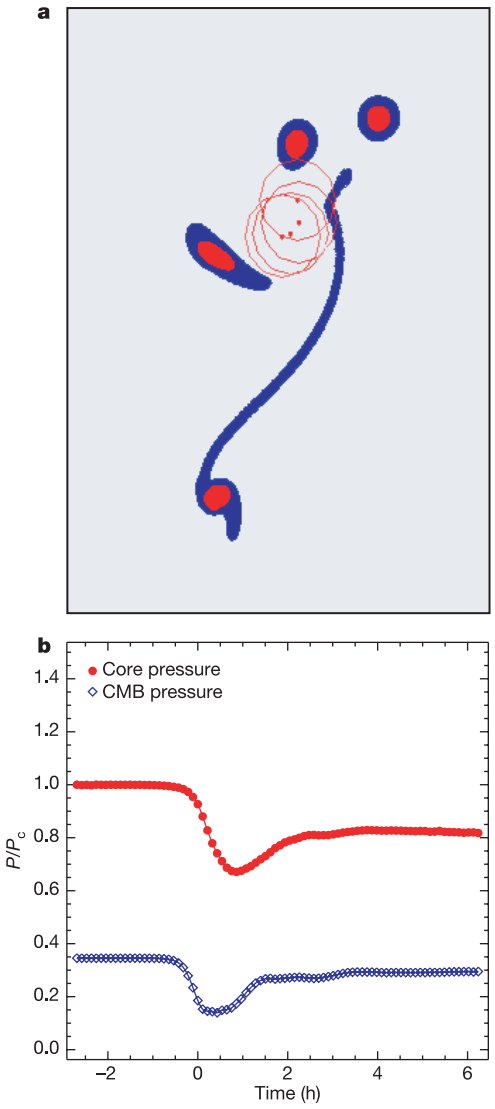

Figure 2 | A Moon-sized differentiated planet ($M = 0.01M_\oplus$) grazing a Mars-sized ($0.1M_\oplus$) planet, resulting in mass loss, spin-up and global pressure unloading. Here $M_\oplus$ is the mass of the Earth. There is no physical contact, only gravitation and unloading. The interloper is a non-rotating, isostatically and thermally equilibrated sphere. Because the interloper does not impact, the central body is modelled as a sphere in this calculation. The closest-approach velocity is $1.05v_{esc}$ and the closest approach distance is $a = 1.05(R + r)$. **a**, The two planets are shown in the centre-of-mass frame, with the larger planet being displaced towards the top of the figure while the smaller planet swings by towards the bottom and is severely deformed. The larger planet is shown as an open red circle, with its centre of mass shown by a red dot; the smaller planet is shown in blue and red, where blue is the mantle rock and red is the iron core, as revealed in this slice through the symmetry plane of the collision. This panel shows a series of 'snapshots' of the event. Deformation is, in this case, largely a consequence of tidal stress, and thus low-density materials in the outer layers are deformed more severely than the denser interior and are partially removed. **b**, Interior pressures versus time are plotted, averaged over the core–mantle boundary (CMB) region (blue line) and over the central core region (red line) of the impactor. Here P is the pressure in each region of the interloper, and P_c is the initial hydrostatic central pressure. The pressure unloads throughout the interloper, by 30–50% for about an hour during periapse, and permanently by about 20% as a result of mass loss and spin-up.

planet is already partially molten. In the removed materials, unloading is permanent and almost total, and equally abrupt—a scenario for phreatic igneous processes discussed below.

For closer, impacting encounters, gravitational stresses increase, and shock and mechanical stresses also become intense. We model impacts using the same SPH technique, starting with two differentiated, equilibrated planets of identical composition and comparable size. Characteristic outcomes (see refs 1, 20) of such collisions are shown in Fig. 3; both involve a Mars-sized target struck at $\xi = 30°$ at typical velocities. In the first scenario (Fig. 3a), the impactor is one-half the target mass and $v_{\rm imp} = 1.5v_{\rm esc}$ (that is, the random relative velocity $v_\infty \approx 1.1v_{\rm esc}$). It emerges more-or-less intact but stripped of its outer layers and spun into fast rotation. Figure 3b shows a faster impactor ($v_{\rm imp} = 2v_{\rm esc}$; $v_\infty \approx 1.7v_{\rm esc}$) one-tenth the target mass which disrupts into a fractionated S–L/9-like chain of fragments, with iron-rich bodies at the centre (shown red) and mantle-rich bodies in the 'wings'. There is no net accretion in either collision; iron fraction is increased in both planets due to mantle loss, most notably from the impactor. A report on the detailed outcomes of hundreds of representative collisions is forthcoming.

Degassing

When impactors and their removed materials depressurize from pre-impact equilibrium conditions, they might degas. Figure 4 shows equilibrium equations of state computed for molten early mantle containing 1, 5 and 10 wt% water—plausible conditions for young planetary embryos. The limited solubility of water in silicate liquids at low pressures means that the mantle of a hot primitive embryo is probably degassed at shallow levels, whereas the deep mantle can retain abundant water. Planetary embryos suffering severe mass loss, spin-up or fragmentation might, according to Fig. 2b, experience a global hydrothermal event in the hours during and following depressurization. According to Fig. 4, a core-mantle pressure drop of 50% in a water-bearing Moon-sized object would initiate extensive deep-mantle degassing. As for materials no longer bound to an impactor (Figs 2a and 3), there is little if any post-encounter pressure support. Removed materials would be almost totally unloaded from their equilibrium pressure, and if molten would efficiently degas throughout—a recipe for dry, igneous, fine-scale meteoritic debris.

Stress accommodation

Unloading from equilibrium pressure requires deformation over the encounter timescale, and there exist conflicting analyses of whether this is possible. SPH simulations similar to those above were used[21] to argue that bulk viscosity prevents tidal disruption, but it was later argued[22] that the use of numerical damping in place of rheological viscosity in those simulations led to artificial resistance to deformation, and that tidal disruption does occur. SPH is not the best tool for studying viscous deformation, so we address this topic with a straightforward geophysical analysis of a viscoelastic impactor succumbing to deformational stresses during the course of a hit-and-run collision. To be conservative, we consider the tidal stresses, apart from shocks and mechanical shears, that can disrupt an impactor.

For incompressible inviscid impactors much smaller than the target, tidal-induced gravitational deformation is invariant with size when distance is normalized to $R_{\rm Roche}$ and time normalized to the gravitational timescale $\tau_{\rm grav}$, or equivalently v_∞ to $v_{\rm esc}$ (ref. 11). Assuming $v_\infty \propto v_{\rm esc}$, the encounter timescale is $\tau_{\rm grav} = (G\rho)^{-1/2}$. The invariance arises because tidal stress scales with $G\rho^2 b^{-3} r^2$, where b is the distance to the target centre-of-mass normalized to $R_{\rm Roche}$, while the overburden stress that is acted against scales with $G\rho^2 r^2$. Real planets also resist deformation through strength and viscosity, in addition to self gravity, but these forces, we now show, are small compared with unloading stresses at the deformation rates expected during late-stage collisions.

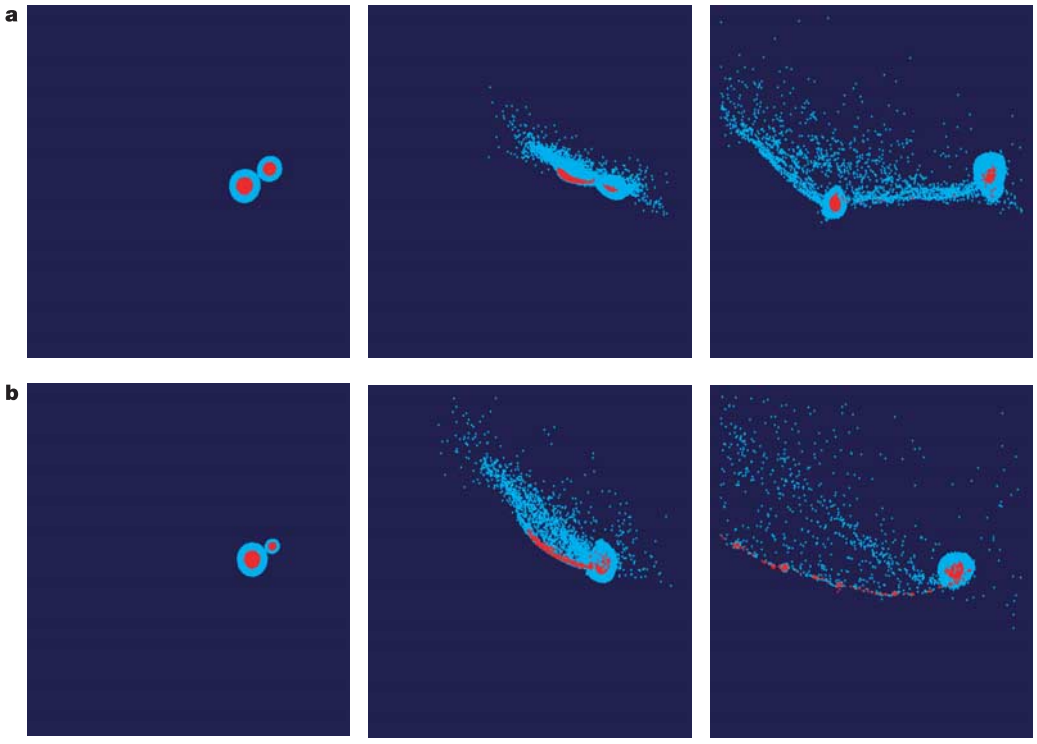

Figure 3 | Two typical collisions involving differentiated planetary embryos. The target mass is $M = 0.10M_\oplus = 5.98 \times 10^{26}$ g and the impactor mass is **a**, $m = M/2$, and **b**, $m = M/10$. Blue is mantle rock and red is core iron, this time showing all SPH particles overplotted. Impact velocities are typical of terrestrial planet formation, **a**, $v = 1.5v_{\rm esc}$ and **b**, $v = 2.0v_{\rm esc}$. Impact angle is $\xi = 30°$ in both cases. The simulations are shown before, during, and 3 h after the impact, in side view. Mantle (blue) is lost in some degree from all major remnants of non-accretionary collisions; in **b**, a chain of iron-enriched bodies derive from the impactor.

Elastic failure

Let $\eta = \eta_{\rm eff}$ be the effective newtonian viscosity at given stress σ_{ij} and temperature T, and E the elastic modulus. If the visco-elastic Maxwell time $\tau_{\rm Maxwell} = \eta/E > \tau_{\rm grav}$, the response is elastic and disruption requires brittle fragmentation. For $E \approx 10^{10}\,{\rm dyn\,cm^{-2}}$ and $\tau_{\rm grav}$ of several hours, elastic response applies for $\eta > 10^{14}$ poise ($1\,{\rm poise} = 1\,{\rm g\,cm^{-1}\,s^{-1}}$), the case we consider first. For a given encounter distance a, tidal stress increases with r^2, where r is the impactor radius; this led to Jeffreys' result[12] that elastic rocks larger than ~200 km fracture during close encounters with Earth.

Interestingly, the brittle unloading of the impactor's equilibrium overburden stress over $\tau_{\rm grav}$ can itself lead to dynamic fragmentation, apart from shock damage. If an elastic mantle obeys Weibull failure statistics, then the number of active flaws per unit volume is $n(\varepsilon) = k\varepsilon^m$, where $\varepsilon = \sigma/E$ and σ is the flaw activation stress. If the characteristic mantle stress $\sigma \approx G\rho^2 r^2$ unloads over $\tau_{\rm grav}$, then the characteristic strain rate is

$$\dot{\varepsilon} = G^{3/2}\rho^{5/2}r^2/E \qquad (1)$$

which gives[23] a characteristic fragment size $L \approx 6c_{\rm g}\alpha^{-1/m+3}\dot{\varepsilon}^{-m/m+3}/(m+2)$, where $\alpha = 8\pi c_{\rm g}^3 k/[(m+1)(m+2)(m+3)]$ and $c_{\rm g}$ is the crack growth velocity, about half the sound speed. Fragment size thus decreases with almost the square of disrupted planet size, as $m \geq 6$ for most geologic materials[24].

Fragmentation also results in response to shear strains whenever part of an impactor is decelerated while another part continues on relatively unimpeded. This shear strain rate can be approximated as the decelerated impact velocity divided by the projectile radius, or $\dot{\varepsilon} = v_{\rm imp}/r$, in which case fragment size decreases approximately linearly with r for a given impact speed. These shear strain rates are in most scenarios much larger than those resulting from stress unloading, and can in principle result in even smaller fragment sizes. But shear strain may be localized, whereas equilibrium unloading is rather uniformly distributed, so unloading establishes the upper limit on expected fragment size. A cold 500-km-diameter basalt sphere ($k = 4 \times 10^{29}\,{\rm cm^{-3}}$, $m = 9$) cracks into ~200-m fragments if unloaded of its equilibrium stress over $\tau_{\rm grav}$, and a 1,000-km sphere cracks into ~70-m fragments. Weibull coefficients for other rocks give comparable sizes. This indicates that no large monoliths survive following the disruption of large solid bodies, even without considering shock damage. Shocks, shears and degassing stresses further comminute unloaded rocky materials. Instant rubble piles form if these new fragments do not disperse, and families of small asteroids form otherwise. This is of relevance to the 'missing mantle' paradox (discussed further below), where mantle material is missing from the meteorite collection and not readily identified among asteroids. One offered explanation[25] is that the excavated mantle rock is fragile and therefore ground down to small sizes by a subsequent collisional cascade—something made easier if fragmentation is a natural outcome of mantle unloading.

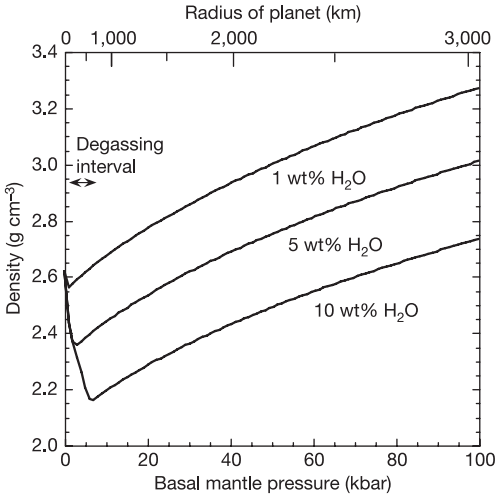

Figure 4 | The pressures at which degassing initiates. These are evaluated for variable water contents, and in terms of the radius of planetesimals containing 30 wt% Fe cores. We calculate the density of silicate melt with $(Mg_{0.9},Fe_{0.1})SiO_3$-composition which is initially at the core–mantle boundary (CMB) pressure. The initial Moon-sized impacting embryo used in the hit-and-run simulations of Figs 2 and 3b plots at $R = 1{,}500$ km. The initial embryo is assumed to be largely undegassed at depth, with water lowering the bulk density relative to the $(Mg_{0.9},Fe_{0.1})SiO_3$ endmember; when mantle is unloaded to below a given value (~6, ~4 and ~2 kbar for 10, 5 and 1 wt% H_2O respectively), the melt becomes oversaturated with water and will begin to degas, increasing the density of the residual melt. The timescale of the pressure unloading (Fig. 2) suggests that degassing will be runaway rather than transitory, as the timescale for bubble nucleation is of the order of 100 s. Density, elasticity and water solubility data are from refs 41–43.

Viscous failure

During late-stage accretion, impact heating and short-half-life radionuclide decay kept embryos hot, perhaps molten, for millions of years; viscous deformation is therefore a more likely scenario for large-scale events. Viscosity decreases with $e^{-T_o/T}$, where T is temperature and T_o a reference temperature. The effects of partial melt and water content markedly increase the strain rates at which silicates deform, and while grain sizes and melt distribution have complex rheologic effects, characteristic shifts in strain rates for even 10% partial melting are well over an order of magnitude under hydrous conditions[26]. For power-law fluids $\dot{\varepsilon} \propto \sigma^n$, and the effective viscosity $\eta_{\rm eff} \propto \sigma^{1-n}$ decreases with about the square of the applied stress ($n \approx 3$ for cold ice and dry quartzite). Effective viscosity is thus low under high differential stress, especially the conditions of planetary unloading.

To disrupt, deformation strain $\varepsilon_{\rm def}$ must accrue over a few times $\tau_{\rm grav}$. As an order of magnitude estimate, let $\varepsilon_{\rm def} \approx 10$ for disruption. The maximum viscosity $\eta_{\rm lim}$ accommodating this deformation is approximately the stress that must be unloaded, $\sigma \approx G\rho^2 r^2$, divided by the required strain rate, $\dot{\varepsilon} \approx \varepsilon_{\rm def}/\tau_{\rm grav}$. The following viscosity thus limits tidal disruption:

$$\eta_{\rm lim} \approx \varepsilon_{\rm def}^{-1}\sqrt{G}\rho^{3/2}r^2 \qquad (2)$$

Viscous strains $\varepsilon_{\rm def} > 10$ accrue when $\eta < \eta_{\rm lim} \approx 10^{12}(r/1{,}000\,{\rm km})^2$ poise ($\rm g\,cm^{-1}\,s^{-1}$). As benchmarks, models of early-Earth convection assume mid-mantle viscosities $\sim 10^9$ poise (ref. 27), and $\eta \approx 10^9$–10^{13} poise is used[28] to model Io's present asthenosphere.

Analyses in viscous and brittle regimes therefore suggest that embryos the size of the largest present asteroids were vulnerable to disruptive deformation from tides alone, let alone impact shocks and disruptive shears, as long as larger 'target' embryos were around. Hit-and-run planetary collisions comparable in scale to the proposed Moon-forming event[8–10] may well have happened on the way to terrestrial planet formation, as they are statistically common for expected impact parameters[1]. The most recognizable signatures of these disrupted and fragmented impactors would then be found primarily among populations where unaccreted relics survive.

Giant impacts in the asteroid belt

The original asteroid belt is believed to have accreted to form bodies with diameters of ~1,000 km (or larger[29]) and then to have dynamically lost most of its mass, thereby 'fossilizing' an early stage of accumulation[30]. Because accretion in the late stage is favoured[1] at low ξ, the 'winners' of accretion (finished planets) tend to consist of shock-processed materials acquired by direct hits, whereas 'losers'—for example, post-accretion asteroid populations—become relatively enriched in unaccreted collisional material forming when bodies of similar size collide. Meteorites that are derived from large, differentiated asteroids are thus expected to contain a mix of relatively unshocked materials worked by gravitational unloading

and mechanical shearing, together with the shocked remnants from direct collisions. As noted above, the small, undifferentiated members of the original asteroid population will not commonly undergo hit-and-run collisions, simply because when $r \ll R$ encounters are either purely tidal, and gentle for these size scales, or else are hypervelocity cratering events (for example, S–L/9).

Disruption, pressure release and fractionation observed in our simulations, and associated hydrothermal activity and possible degassing, can be related to an array of quandaries[25,31–34] regarding meteorites deriving from large parent bodies. One straightforward puzzle is the apparent absence of mantle-derived meteorites ($\lesssim$1% of non-chondritic falls) when so many irons and stony-irons have been excavated from core regions ($\gtrsim$10% of non-chondritic falls). The major volume of these disrupted planets appears absent. This is answered in two ways by the models presented above. First, liberated mantle, if brittle, is fragmented by unloading to relatively small sizes (equation (1)). If hot and viscous (equation (2)), liberated mantle rocks are likely to be melted by unloading and hydrothermally altered as water exsolves, and might not be recognizable as mantle rock. Second, the global mechanical shearing suffered by an impactor greatly increases the surface area of the core–mantle boundary during a hit-and-run collision (for example, Fig. 3b), thereby mixing iron and silicate and increasing the abundance and diversity of stony-iron meteorites.

A related puzzle is how to remove entire mantles from some differentiated asteroids while preserving others. No fewer than 10 and as many as 100 distinct iron reservoirs, presumably embryonic cores, are sampled by iron meteorites (ref. 24 and references therein). A number of large M-class asteroids (for example, 216 Kleopatra[35] and 16 Psyche) are believed to be metallic, as are most smaller M-class asteroids[36]. A serious problem arises if impact is used to excavate iron from the cores of so many asteroids, because it becomes statistically impossible for the 530-km-diameter main-belt asteroid 4 Vesta to preserve its signature basaltic crust[37] while neighbouring asteroids are stripped bare. Even if Vesta managed to dodge all catastrophic impactors, any impacting population includes a power-law distribution of smaller sizes[38], so Vesta must also have dodged myriad subcatastrophic collisions that would scramble, if not disperse, its basaltic crust.

Explaining Vesta's surviving crust, while accommodating widespread asteroid mantle removal, appears intractable. However, if these metallic asteroids and associated remnants began as one or more impactors disrupted by larger targets (for example, the disrupted interloper in Fig. 3b) and not vice versa, then Vesta only had to avoid collisions with larger bodies until any Moon-sized or larger embryos were ejected from the main belt[29]. The corollary is that meteoroids massive and energetic enough to catastrophically disrupt Vesta-sized asteroids were relatively rare, and that Vesta's bombardment experience (one hemispheric impact basin formed over its history[39]) is typical rather than unusually lucky.

A third puzzle is the evidence for widespread global melting of asteroids on the basis of oxygen isotope homogenization in meteorite parent bodies[40]. It has been rightly argued[33] that impacts are inefficient at global heating of asteroids, because impact shock can only deliver so much heat before disrupting and dispersing a body of this size, and because shock heating is local. Global melting of asteroids by short-lived radionuclide decay is even more controversial, given the critical timing constraints. Gravitational unloading can melt a body by pressure release throughout its deep interior, a process warranting more detailed examination on the basis of our studies so far.

Discussion

We have revisited planetary giant impacts from the perspective of the impactor, and identify an additional scenario for asteroid formation and planetary evolution where the smaller body is disrupted by the larger. This mode of disruption is complex, and some of the thermophysical effects (pressure unloading and removal of the outer layers) require more detailed exploration. But owing to the prevalence of 'hit and run' collisions at expected encounter geometries and velocities[1], the products of impactor disruption are likely to be common among unaccreted planetary populations—asteroids, meteorites and perhaps the smallest planets.

Received 13 July; accepted 6 October 2005.

1. Agnor, C. & Asphaug, E. Accretion efficiency during planetary collisions. *Astrophys. J.* **613,** L157–L160 (2004).
2. Wetherill, G. W. Occurrence of giant impacts during the growth of the terrestrial planets. *Science* **228,** 877–879 (1985).
3. Agnor, C. B., Canup, R. M. & Levison, H. F. On the character and consequences of large impacts in the late stage of terrestrial planet formation. *Icarus* **142,** 219–237 (1999).
4. Greenberg, R., Hartmann, W. K., Chapman, C. R. & Wacker, J. F. Planetesimals to planets—Numerical simulations of collisional evolution. *Icarus* **35,** 1–26 (1978).
5. Weidenschilling, S. J., Spaute, D., Davis, D. R., Marzari, F. & Ohtsuki, K. Accretion evolution of a planetesimals swarm. *Icarus* **128,** 429–455 (1997).
6. Kokubo, E. & Ida, S. Formation of protoplanetary systems and diversity of planetary systems. *Astrophys. J.* **581,** 666–680 (2002).
7. Pierazzo, E. & Melosh, H. J. Hydrocode modelling of oblique impacts: The fate of the projectile. *Meteorit. Planet. Sci.* **35,** 117–130 (2000).
8. Stevenson, D. J. Origin of the moon—The collision hypothesis. *Annu. Rev. Earth Planet. Sci.* **15,** 271–315 (1987).
9. Canup, R. M. Dynamics of lunar formation. *Annu. Rev. Astron. Astrophys.* **42,** 441–475 (2004).
10. Canup, R. & Asphaug, E. Origin of the Moon in a giant impact near the end of the Earth's formation. *Nature* **412,** 708–712 (2001).
11. Asphaug, E. & Benz, W. Size, density, and structure of comet Shoemaker-Levy 9 inferred from the physics of tidal breakup. *Icarus* **121,** 225–248 (1996).
12. Jeffreys, H. The relation of cohesion to Roche's limit. *Mon. Not. R. Astron. Soc.* **107,** 260–262 (1947).
13. McKinnon, W. B. & Schenk, P. M. Estimates of comet fragment masses from impact crater chains on Callisto and Ganymede. *Geophys. Res. Lett.* **22,** 1829–1832 (1995).
14. Boss, A. P., Cameron, A. G. W. & Benz, W. Tidal disruption of inviscid planetesimals. *Icarus* **92,** 165–178 (1991).
15. Rettig, T. W., Mumma, M. J., Sobczak, G. J., Hahn, J. M. & DiSanti, M. The nature of Comet Shoemaker-Levy/9 subnuclei from analysis of preimpact Hubble Space Telescope images. *J. Geophys. Res.* **101,** 9271–9281 (1996).
16. Abe, Y., Ohtani, E., Okuchi, T., Righter, K. & Drake, M. in *Origin of the Earth and Moon* (eds Canup, R. & Righter, K.) 413–433 (Univ. Arizona Press, Tucson, 2000).
17. Wilson, L. Relationships between pressure, volatile content and ejecta velocity in three types of volcanic explosion. *J. Volcanol. Geotherm. Res.* **8,** 297–313 (1980).
18. Jeans, J. H. *Problems of Cosmogony and Stellar Dynamics* (Cambridge Univ. Press, Cambridge, 1919).
19. Benz, W. in *The Numerical Modeling of Nonlinear Stellar Pulsations: Problems and Prospects* (ed. Buchler, J. R.) 269–288 (Kluwer Academic, Boston, 1990).
20. Asphaug, E., Agnor, C. & Williams, Q. Tidal forces as drivers of collisional evolution. *Lunar Planet. Sci. Conf.* **XXXVI** abstr. 2393 (2005); ⟨http://www.lpi.usra.edu/meetings/lpsc2005/pdf/2393.pdf⟩ (2005).
21. Mizuno, H. & Boss, A. P. Tidal disruption of dissipative planetesimals. *Icarus* **63,** 109–133 (1985).
22. Sridhar, S. & Tremaine, S. Tidal disruption of viscous bodies. *Icarus* **95,** 86–99 (1992).
23. Grady, D. E. & Kipp, M. E. Continuum modeling of explosive fracture in oil shale. *Int. J. Rock Mech. Min. Sci. Geomech. Abstr.* **17,** 147–157 (1980).
24. Asphaug, E., Ryan, E. & Zuber, M. in *Asteroids III* Table I (eds Bottke, W. F. Jr, Cellino, A., Paolicchi, P. & Binzel, R. P.) 463–484 (Univ. Arizona Press, Tucson, 2002).
25. Burbine, T. H., Meibom, A. & Binzel, R. P. Mantle material in the main belt: Battered to bits? *Meteoritics* **31,** 607–620 (1996).
26. Mei, S., Bai, W., Hiraga, T. & Kohlstedt, D. L. Influence of melt on the creep behaviour of olivine-basalt aggregates under hydrous conditions. *Earth Planet. Sci. Lett.* **201,** 491–507 (2002).
27. Walzer, U., Hendel, R. & Baumgardner, J. The effects of a variation of the radial viscosity profile on mantle evolution. *Tectonophysics* **384,** 55–90 (2004).
28. Tackley, P. J. Convection in Io's asthenosphere: Redistribution of nonuniform tidal heating by mean flows. *J. Geophys. Res.* **106,** 32971–32982 (2001).
29. Wetherill, G. W. An alternative model for the formation of the asteroids. *Icarus* **100,** 307–325 (1992).
30. Bottke, W. F. *et al.* The fossilized size distribution of the main asteroid belt. *Icarus* **175,** 111–140 (2005).
31. McCoy, T. J. *et al.* A petrologic and isotopic study of Iodranites: Evidence for early formation as partial melt residues from heterogeneous precursors. *Geochim. Cosmochim. Acta* **61,** 623–637 (1997).

32. Haack, H., Scott, E. R. D. & Rasmussen, K. L. Thermal and shock history of mesosiderites and their large parent asteroid. *Geochim. Cosmochim. Acta* **60,** 2609–2619 (1996).
33. Wilson, L., Keil, K., Browning, L. B., Krot, A. N. & Bourcier, W. Early aqueous alteration, explosive disruption, and re-processing of asteroids. *Meteorit. Planet. Sci.* **34,** 541–557 (1999).
34. Keil, K., Stöffler, D., Love, S. G. & Scott, E. R. D. Constraints on the role of impact heating and melting in asteroids. *Meteoritics* **32,** 349–363 (1997).
35. Ostro, S. J. *et al.* Radar observations of asteroid 216 Kleopatra. *Science* **288,** 836–839 (2000).
36. Rivkin, A. S., Howell, E. S., Lebofsky, L. A., Clark, B. E. & Britt, D. T. The nature of M-class asteroids from 3-μm observations. *Icarus* **145,** 351–368 (2000).
37. Davis, D. R., Chapman, C. R., Greenberg, R. & Weidenschilling, S. J. Collisional history of asteroids: Evidence from Vesta and the Hirayama families. *Icarus* **62,** 30–53 (1985).
38. Dohnanyi, J. W. Collisional models of asteroids and their debris. *J. Geophys. Res.* **74,** 2531–2554 (1969).
39. Binzel, R. P. *et al.* Geologic mapping of Vesta from 1994 Hubble Space Telescope images. *Icarus* **128,** 95–103 (1997).
40. Greenwood, R. C., Franchi, I. A., Jambon, A. & Buchanan, P. C. Widespread magma oceans on asteroidal bodies in the early Solar System. *Nature* **435,** 916–919 (2005).
41. Rivers, M. L. & Carmichael, I. S. E. Ultrasonic studies of silicate melts. *J. Geophys. Res.* **92,** 9247–9270 (1987).
42. Ochs, F. A. III & Lange, R. A. The density of hydrous magmatic liquids. *Science* **283,** 1314–1317 (1999).
43. Dixon, J. E., Stolper, E. M. & Holloway, J. R. An experimental study of water and carbon dioxide solubilities in mid-ocean ridge basaltic liquids. Part I. Calibration and solubility models. *J. Petrol.* **36,** 1607–1631 (1995).
44. Benz, W. & Asphaug, E. Catastrophic disruptions revisited. *Icarus* **142,** 5–20 (1999).

Acknowledgements This research was sponsored by NASA's Planetary Geology and Geophysics Program, "Small Bodies and Planetary Collisions". We benefited from discussions with a number of colleagues, including W. F. Bottke and R. Canup. We particularly thank D. Stevenson and K. Zahnle for comments on the manuscript.

Author Information Reprints and permissions information is available at npg.nature.com/reprintsandpermissions. The authors declare no competing financial interests. Correspondence and requests for materials should be addressed to E.A. (asphaug@pmc.ucsc.edu).